

# A New Catalog of HII Regions in M31

M. Azimlu, R. Marciniak, & P. Barmby

*Department of Physics & Astronomy*

*University of Western Ontario*

*1151 Richmond St., London, ON N6A 3K7 Canada*

## ABSTRACT

We present a new catalog of HII regions in M31. The full disk of the galaxy ( $\sim 24$  kpc from the galaxy center) is covered in a  $2.2 \text{ deg}^2$  mosaic of 10 fields observed with the Mosaic Camera on the Mayall 4 m telescope as part of the Local Group Galaxies survey. We used HIIPhot, a code for automated photometry of HII regions, to identify the regions and measure their fluxes and sizes. A  $10\sigma$  detection level was used to exclude diffuse gas fluctuations and star residuals after continuum subtraction. That selection limit may result in missing some faint HII regions, but our catalog of 3691 HII regions is still complete to a luminosity of  $L_{H\alpha} = 10^{34} \text{ erg s}^{-1}$ . This is five times fainter than the only previous CCD-based study which contained 967 objects in the NE half of M31. We determined the  $H\alpha$  luminosity function (LF) by fitting a power law to luminosities larger than  $L_{H\alpha} = 10^{36.7}$  and determined a slope of  $2.52 \pm 0.07$ . The in-arm and inter-arm LFs peak at different luminosities but they have similar bright-end slopes. The inter-arm regions are less populated (40% of total detected regions) and constitute only 14% of the total luminosity of  $L_{H\alpha} = 5.6 \times 10^{40} \text{ erg s}^{-1}$  (after extinction correction and considering 65% contribution from diffused ionized gas). A star formation rate of  $0.44 \text{ M}_{\odot} \text{ yr}^{-1}$  was estimated from the  $H\alpha$  total luminosity; this value is consistent with the determination from the *Spitzer*  $8 \mu\text{m}$  image. We removed all known and potential planetary nebulae, yet we found a double peaked luminosity function. The inter-arm older population suggests a starburst between 15 and 20 million years ago. This result is in agreement with UV studies of the star formation history in M31 which found a star formation rate decrease in the recent past. We found a fair spatial correlation between the HII regions and stellar clusters in selected star forming regions. Most of the matched regions lie within the arm regions.

## 1. Introduction

Dense clumps in giant molecular clouds are the birthplaces of stars in galaxies. Most of the newborn stars are embedded within dense cores and obscured by dust. Only massive stars can heat the gas and dust in their environs by emitting ultraviolet (UV) photons and ionizing the surrounding hydrogen, producing HII regions. The ionized gas radiates mostly in the  $H\alpha$  line, therefore photometry and spectroscopy of  $H\alpha$  emission is one of the main probes of local and global star formation in nearby galaxies. HII regions are one of the best-known massive star formation tracers in other galaxies (e.g. Kennicutt et al. 2008; Thilker et al. 2000; Lawton et al. 2010). They might be excited by only one star or multiple young massive stars or even clusters. Properties of HII regions such as shape, size, distribution and abundances vary with the physical characteristics of the ionizing stars, galaxy type, and environmental conditions such as gas density and metallicity (Hodge & Kennicutt 1983; Kennicutt 1984; Elmegreen & Hunter 2000; Thilker et al. 2002; Esteban et al. 2009).

HII regions are observed to have a wide range of size and luminosities. For example 30 Doradus (size  $\sim 300$  pc) in the Large Magellanic Cloud (LMC) is the largest known HII region in the Local Group and is excited by a cluster of massive stars with a total stellar mass of  $0.35 - 1 \times 10^5 M_{\odot}$  (Campbell et al. 2010). In comparison, a typical Galactic HII region is excited by an individual B star and can be smaller than a parsec.

The characteristics of HII regions have been studied in many extragalactic  $H\alpha$  surveys [e.g. Knapen (1998) and references therein; Petit et al. (1998); Thilker et al. (2002); Kennicutt et al. (2008)]. The studies by Kennicutt (1988) and Kennicutt et al. (1989, KEH89 hereafter) of the population of HII regions in nearby galaxies confirmed that HII region population properties are strongly dependent on the host galaxy Hubble type. The massive star formation rate and the frequency of giant HII regions are noticeably higher in late type galaxies.

The star formation properties of galaxies can be determined through study of their numerous HII regions (Walterbos & Braun 1992, WB92 hereafter). From the  $H\alpha$  flux one can determine the number of Lyman continuum photons (Spitzer 1978), which in turn is used to determine the mass of the ionizing stellar population, providing an upper limit to the initial mass function (IMF) for massive stars (Oey et al. 2003). Since the amount of  $H\alpha$  luminosity depends on the ionizing flux of the young O and B stars, we expect that the HII regions' luminosity function (LF) should also trace the distribution of ionizing stellar masses (Oey et al. 2003). The LF can be well fitted for all galaxies by a power law function but the slope varies with galaxy Hubble type (KEH89). The HII regions are mostly located within the arms of spiral galaxies but the LF for in-arm and inter-arm regions might be different (e.g. Thilker et al. 2000). A Monte Carlo simulation to study the evolution of

HII LFs (Oey & Clarke 1998) suggested that arm populations represent the current active star forming regions while inter-arm regions are aged populations. However this method of studying the stellar populations only gives accurate measurements for luminous massive stars in nearby and face-on galaxies. The size distribution of HII regions in a galaxy can also be compared between galaxies as a structural property (van den Bergh 1981).

M31 is the nearest large galaxy to our own and can be studied in great detail. Baade & Arp (1964) made the first catalog of the position of emission nebulae in M31. The study was followed by that of Arp (1973), who measured the size of the largest extended regions in M31 and M33. The most recent complete catalog of HII regions in M31 was produced by Pellet et al. (1978). That study had a spatial resolution of  $4''$  ( $\sim 15$ pc) and detected 981 HII regions. WB92 made the first deep CCD images of the North-East half of the galaxy in the  $H\alpha$  and  $[SII]$  emission lines. They imaged 19 fields, each covering a  $6.6 \text{ arcmin}^2$  area (the largest possible field of view at the time), trying to cover the most active star forming regions in the North-East half of M31. They measured and calculated the positions, dimensions and fluxes of 967 HII regions.

The complicated morphology of M31 suggests a violent history. A star forming ring with radius of 10 kpc which is not centered at the galaxy nucleus (Gordon et al. 2006), and a second inner dust ring 0.5 kpc from the center (Block et al. 2006) suggest past collisions. Other features such as tidal streams (e.g. Ibata et al. 2001; Fardal et al. 2008) indicate active interactions between M31 and other Local Group members.

We study the properties of the spatially resolved HII regions in M31 and try to connect these to present and past star formation processes in the galaxy. In this work we present a new catalog of HII regions over the entire disk of M31, using higher resolution ( $1''$ ,  $\sim 3.8$  pc)  $H\alpha$  imaging (Massey et al. 2006). We identified 3961 distinct regions to a limiting size of  $4.08''$  (15.6 pc) and limiting detection flux of  $\sim 10^{-16} \text{ erg cm}^{-2} \text{ s}^{-1}$ . Throughout this work we assume a distance to M31 of 0.783 Mpc (Mochejska et al. 2000).

Details of the data set, data reduction and data analysis methods including the HIIphot code parameters setting are provided in §2. In §3, we introduce the characteristics of the new catalog of HII regions in M31 and compare it with previous works. In §4 we derive the luminosity function, total  $H\alpha$  luminosity, size distribution, and match our catalog with young stellar clusters in M31. §5 contains a summary of our results.

## 2. Data Analysis

The data used came from the Nearby Galaxies Survey of Massey et al. (2006) and were obtained from the NOAO science archive. The images were taken at the 4 m Mayall telescope with the Mosaic CCD Camera between August 2000 and September 2002 and comprise H $\alpha$  and R band mosaics of ten overlapping fields across the disk of M31. The new images permit photometry with negligible uncertainty to an H $\alpha$  magnitude of 20 and have delivered image quality varying between 0.9'' and 1.4'' (equivalent to 3.4–5.3 pc). Each field has an approximate angular size of 36'  $\times$  36' observed as a set of 5 dithered exposures, while the entire survey covered 2.2 square degrees of M31. The pixel scale is 0''.258 pixel<sup>-1</sup>, with an average PSF FWHM of 1'' ( $\approx$ 4 pixels). The accuracy of the astrometric calibration is not discussed by Massey et al. (2006), although the discussion in Massey et al. (2007) implies that it is likely to be good to 0''.1. That paper also states that photometric calibration goal for the narrow-line imaging was a precision of 5–10%, although it is not entirely clear from the discussion whether that goal was reached.

Figure 1 shows the observed fields in dashed rectangles. A 10'  $\times$  10' central region was partially saturated in the images and was omitted from our survey. The black dots show the detected HII regions in our survey with luminosities  $\geq 10^{36}$  erg s<sup>-1</sup>. Red dots are regions fainter than this limit but with a flux uncertainty smaller than 20%. Grey dots present the remained faint regions. The higher luminosity regions clearly trace the spiral arms while the lower luminosity regions fill up the inter-arm spaces as well. We discuss the HII regions' spatial distribution in more detail in §4.5.

Making continuum-subtracted images requires removal of the stellar emission from the H $\alpha$  images using the R band image of the same field. To make the subtraction we have to assume that all stars have the same H $\alpha$  fraction in their spectra. This is not accurate as different spectral types have different absorption line depths for H $\alpha$ , and what is being measured is the best fit H $\alpha$  fraction so that most stars are properly removed. Some residuals will be present due to variations in spectral shape and absorption line depths from star to star. To perform the subtraction the amount of continuum emission present in each H $\alpha$  image must be determined. We used SExtractor to obtain the photometry of stars in H $\alpha$  and R bands. A scaling factor between H $\alpha$  and R fluxes was then obtained by comparing fluxes of the bright stars. All the images had nearly a linear relation between the two bands with similar slopes (scaling factor) of 0.36 to 0.41; Field 2 was an exception, with a scaling factor of 0.86. This field was reported by Massey et al. (2006) to have a flatness problem which resulted in a slightly different color, so the different scaling factor is not unexpected. The H $\alpha$  and R images are aligned on the same coordinate grid, so for each field the continuum-subtracted H $\alpha$  image was constructed by subtracting the R-band image multiplied by the

scaling factor from the  $H\alpha$  image. The scaling factors are reported in Table 1 for the benefit of future users.

Calibration of the Nearby Galaxies Survey images is the final step before running HIIPhot. HIIPhot requires that the continuum-subtracted image be in units of emission measure (EM). We convert from image units to EM in  $\text{pc cm}^{-6}$  using the image exposure time (300 s), the calibration factor given by Massey et al. (2007) (and the correction to its units given by Relaño & Kennicutt 2009), the average pixel scale of  $0''.258$ , and the  $H\alpha$ -to-EM conversion ratio as used in the HIIPhot code of  $2.0 \times 10^{-18} \text{ erg cm}^{-2} \text{ s}^{-1} \text{ arcsec}^{-2} \text{ pc}^{-1} \text{ cm}^6$ . Combining these factors gives an overall conversion factor from ADU to EM of 4.437. We also need to account for the flux contribution to the  $H\alpha$  filter from the  $[\text{NII}]$  6583 Å line. The  $[\text{NII}]$  percentage is given as the fraction of  $[\text{NII}]$  present in the filter band pass multiplied by the relative intensity of the  $[\text{NII}]$  line compared to  $H\alpha$ . James et al. (2005) studied 334 nearby galaxies and found that  $[\text{NII}]$  emission is not distributed exactly the same as the  $H\alpha$  emission. Therefore the  $I[\text{NII}]6583/I[H\alpha]$  ratio varies within a galaxy, particularly in nuclear regions and also with galaxy type. Greenawalt et al. (1997a), however, reported that in diffuse ionized gas (DIG) near HII regions, the intensity ratio  $I[\text{NII}]6583/I[H\alpha] = 0.35$  and we use this value for the  $[\text{NII}]$  contribution to the total detected emission.

## 2.1. Running HIIPhot

HII regions come in a large range of sizes and shapes. The characteristics of HII regions depend on the exciting stars, the ionizing photons they emit and on the environment in which the stars are ionizing. Therefore HII region photometry is more difficult than stellar photometry. The physical extent of regions are not well defined, and borders between regions and emission from DIG are difficult to distinguish. Different methods and algorithms have been used to identify the HII regions, define the boundaries, subtract the background emission and measure the flux in various studies from hand works to detailed sensitive computer codes (e.g. Pellet et al. 1978; Knapen et al. 1993; Walterbos & Braun 1994; Knapen 1998; Rozas et al. 1999; Pleuss et al. 2000; Scoville et al. 2001; James et al. 2004; Gutiérrez et al. 2011). HIIPhot is an IDL code which was developed by Thilker et al. (2000) for the sole purpose of performing accurate photometry of HII regions in external galaxies. Thilker et al. (2000) applied this method to the spiral galaxy M51 and compared their resulting LF to that of Rand (1992), showing that HIIPhot can successfully and accurately reproduce and improve upon existing LFs.

The detailed operation of HIIPhot is described by Thilker et al. (2000); here we give a brief summary. HIIPhot proceeds in an iterative fashion.

An appropriately-sized Gaussian fit is assigned to each local maximum of the data to remove source structure on smaller scales. Following this initial detection of sources, HIIphot assigns *footprints* to these flux peaks, and considers as possible detections only those Gaussian peaks are a specified multiple of the image noise. This multiple is called “S/N” in the HIIphot input parameters, but this “detection signal-to-noise” is not exactly equivalent to the conventional definition as an object’s flux divided by its flux uncertainty. We determined the noise by integrating and averaging over the entire image, rather than a selected empty region, to make sure we did not underestimate the noise in crowded regions or bright regions adjacent to the bulge.

After defining footprints and refining a list of regions, all pixels below 50% of the footprints median flux are rejected, creating seeds, which are a starting point for region growth. Iterative growth proceeds in a manner where the region boundary only expands to adjacent pixels that are above a threshold level. If the pixels are below the threshold they are ignored until a later iteration. If less than 50% of the boundary pixels are above the threshold, the region will not expand during the given iteration. A region’s growth ceases when its surface brightness profile slope flattens to below a user-specified threshold, or when it is completely surrounded by other region boundaries and cannot claim any more pixels.

Preparing the images carefully is critical in order for the code to produce reasonable results with a reasonable amount of computing time. For example, in test runs with S/N=5, stellar residuals left over from the continuum subtraction process accounted for around 80% of total detections. We found that masking isolated stellar sources greatly reduced the run time. A source was determined to be isolated if the flux in an annulus around it was comparable to the background flux in the image: masking only isolated stars ensured that HII region emission fluxes and sizes were not affected. The masked region around each star was a circle with size determined by the original continuum flux of the star, as brighter field stars leave larger residuals. After applying this correction the number of false detections decreased to approximately 20% for S/N=5 and less than 1% for S/N=10. We found that the original images required too much memory to be processed all at once; images for each field were cropped into 8 smaller segments with 250 pixel overlaps to make sure all large areas of H $\alpha$  emission were within a single segment. Duplicate objects detected in more than one segment were removed from the final catalog.

The results of the HIIphot code are sensitive to many factors that determine both the specific results and the computing time needed to run the code. The 20 input parameters required for HIIphot determine the range in HII region model sizes, the resulting fluxes, and the physical extent of region growth i.e. the definition of the boundary between region emission and surrounding DIG. The distance to the galaxy is well established at 0.783 Mpc,

as reported by Mochejska et al. (2000). The coordinates for the noise estimates were taken as the entire images. This results in an overestimate for the noise due to inclusion of bright regions in the averaging. However, the noise estimate is used for locating regions, and not in the flux determination, so the slight overestimate actually reduces the number of false detections due to isolated DIG. The last few input parameters describe the growth of regions, specifically the stopping point for growth in EM pc<sup>-1</sup>. We adopt a value of 1.5 EM pc<sup>-1</sup> for this terminal gradient, keeping consistency with the stopping point of Thilker et al. (2000), described as the boundary between the HII region and the surrounding DIG.

Different S/N and PSF detection limits were tested and the resulting luminosity and size distributions and individual luminosities were compared with WB92. Two different sample fields, one at the edge of the galaxy (sub-field of F1) and one at the center (sub-field of F5) were selected for the test runs. We found that increasing the S/N detection limit with the same PSF decreased the number of detected faint regions but did not affect the LF slope, because all the faint regions had luminosities smaller than the turnover peak used to determine the LF. On the other hand, decreasing the PSF-FWHM with the same S/N resulted in fewer bright regions (they were broken into smaller sub-regions) and resulted in a steeper LF. The detection of image artifacts, such as rings around star residuals, was sensitive to the PSF detection setting as well. We finally chose a PSF-FWHM of 8 pixel equivalent to 7.8 pc (twice the average PSF, the minimum acceptable size for a resolved HII region) and a high S/N of 10 to completely remove the false detections of stars residuals that were not picked up by either the continuum subtraction or the masking code. More importantly, this setting prevented HIIphot from breaking larger regions with some flux fluctuations into false smaller regions.

It is worth noting that defining the borders of HII regions in complexes is not a well-defined problem. There is no consensus on whether HII complexes should be considered as giant HII regions or be broken into smaller regions and if so into what scales. An automated system such as HIIphot still depends on the aperture definitions but reduces the manual selection bias. In our runs we chose parameters which improved the reliability of the final catalog, at the cost of some incompleteness at the faint end. The number of missed regions above the detection limit changes by 10 – 20% in different fields by selecting S/N=10 instead of S/N=5. The missed regions are responsible for less than 5% of the total detected flux, but considering a higher S/N also affects the region edge definition and causes differences in measured fluxes up to 20%. However, most of the neglected flux is from DIG and not to be considered as part of the total H $\alpha$  flux from HII regions.

Background fluctuations and DIG around complexes and in filamentary structures increase the uncertainty in flux measurements. We reiterate that there is a difference between

detection S/N and the flux uncertainty measurement. To calculate the noise we adopt the entire field, rather than the empty regions, as background; this results in a conservative estimate of the noise level. Any source with a signal 10 times larger than this field noise is considered a detection. After growing regions, HIIphot considers the local background in measuring the flux and its uncertainty. As a result the flux uncertainty for regions with high-intensity DIG, large background fluctuations, or regions adjacent to the galaxy center might be noticeably large. A large flux uncertainty does not mean a poor detection. As shown in Figure 2 from Field 7, all the detected sources are real. The source number N1017 in the left panel is the one in Table 2 with the largest flux uncertainty. Another source, N1020, also appears to be real but is not counted as a detection. The other source in the bottom left corner has been matched with a planetary nebula and has been removed from the final catalog. In the final catalog we have removed regions with flux uncertainties larger than 80%. In total only 6% of the remaining regions have a flux uncertainty larger than 50% and only 13% have flux uncertainties larger than 30%. Almost 75% of the regions have flux uncertainties smaller than 20%. The right panel of Figure 2 shows another example of a high flux uncertainty region in Field 4, near the galaxy centre. It lies over an extensive DIG filament, which is why HIIphot was not able to determine an accurate flux. The object is a real compact source. There are several other extended regions or DIG features in the field marked by arrows, which have not been detected as HII regions.

### 3. Final catalog characteristics

Our new catalog contains about 5 times as many regions as the catalogs of Pellet et al. (1978) and WB92. However, those catalogs contain many regions whose diameters are much larger than the largest ( $\sim 190$  pc diameter) region from our catalog. The obvious reason is that our increased spatial resolution, and use of the HIIphot automated detection method, results in many of their largest regions being resolved as complexes of several smaller regions. Figure 3 shows a sample sub-map, comparing our HIIphot detected regions with those of WB92. Black borders are those determined by HIIphot while WB92 regions are presented with white ellipses. The region WB267 has been divided into 22 distinct regions in our catalog. HIIphot also avoids overlap, such as for the regions WB267/WB268 or WB280/WB281, which gives better flux estimates.

We set a high detection limit of  $10\sigma$  in our survey, yet we can detect  $\text{H}\alpha$  emission as faint as  $\sim 10^{-16}$  erg cm $^{-2}$  s $^{-1}$  or a luminosity of  $10^{34}$  erg s $^{-1}$  which is a factor of 5 fainter than WB92. With that luminosity detection limit we can easily pick out the B0 stars but cannot go far beyond to B1 stars.



HII regions are not the only  $H\alpha$ -emitting sources which are detected in our survey. Planetary nebulae (PNe) also emit in  $H\alpha$  and may make up a fraction of the detected objects (Meyssonnier et al. 1993). Ciardullo et al. (1989) suggested that there is a natural limit for the [OIII] luminosity of the brightest PNe. WB92 used that limit to find the maximum  $H\alpha$  luminosity of PNe in M31. Corrected to the new distance for M31, any object which has an  $H\alpha$  luminosity smaller than  $\sim 5 \times 10^{35} \text{ erg s}^{-1}$  could be a PN. To remove the possible PNe detected as HII regions, we matched our catalog with a list of 723 PNe in M31 which covers both disk and bulge of the galaxy (Halliday et al. 2006). We found 374 matches, but 18 of them were brighter than the maximum limit and were not considered. However the detected flux from these regions is partially contributed by the PNe. The remaining unmatched PNe are either out of our field, too faint to be detected, or removed with star residuals. The matched and removed PNe were responsible for 1% of the total measured  $H\alpha$  emission.

Merrett et al. (2006) presented a catalog of 3300 emission-line objects found by the Planetary Nebula Spectrograph in a survey of the Andromeda galaxy. After removing extended objects which are probably HII regions or background galaxies, 2049 of these objects covering a large area beyond the galaxy’s disk were found to be likely PNe. We matched our PNe-removed catalog with this list and found 407 common objects which are mostly compact sources. We did not include these objects in our final catalog and analysis but have listed them in Table 3.

The final catalog contains 3961 HII regions. It contains about 5 times more regions than WB92 which covered only the northeast half of the galaxy. The luminosity limit is also five times fainter with  $L_{H\alpha} = 10^{34} \text{ erg s}^{-1}$ . The average flux uncertainty is  $\sim 5\%$  but it increases in crowded regions with substantial background and especially for faint regions within an extensive background DIG. We removed all the regions with flux uncertainties larger than 80% from the final catalog. 75% of the remaining regions have final flux uncertainty less than 20% and they are responsible for about 97% of the total detected flux.

For each region, the reported position is the coordinates of the flux peak, which is not necessarily at the geometric center of the object especially for irregular morphologies. The typical peak-to-geometric-center separations range from a few up to 10 arcsec. A sample of the final results is presented in Table 2. The full data set is available in the electronic version of the paper and contains the position, dimensions (FWHM major and minor axis in arcsec and full diameter in parsec), position angle,  $H\alpha$  flux, extinction, and extinction-corrected luminosity of the regions.

### 3.1. Comparison with previous catalogs

We compared our  $H\alpha$  fluxes with matched regions from WB92 to check the accuracy of our measurements. To find the best match we considered that many bright complexes detected as one region in WB92 were resolved into smaller fainter regions in our study. Therefore such detections, especially in crowded regions which made the comparison of total fluxes complicated, were excluded. There were also plenty of individual faint regions matched in both catalogs but they were under or close to the resolution limit with larger uncertainties in flux determination and were excluded as well. Finally we found 49 regions well matched in coordinate space, not contaminated by neighbours due to poor resolution, and luminous enough to be well above the detection limit. Figure 4 shows our measured fluxes versus WB92. The grey dots show all the matched regions with a separation  $\leq 0.5''$  and black dots present only extended ( $\geq 12$  pixels, 11.75 pc) well resolved regions. There is more scatter for larger fluxes but an average ratio of  $1.00 \pm 0.12$  is very satisfying. Most of the scatter for larger fluxes results from the difference in edge finding and background correction especially in crowded regions in the spiral arms.

The fact that M31 does not have very luminous HII regions such as 30 Doradus ( $\log(L_{H\alpha}) = 40.17$ ; Kennicutt 1984) in the LMC and NGC604 ( $\log(L_{H\alpha}) = 39.49$ ; Relaño & Kennicutt 2009) in M33 was addressed before (KEH89, WB92). These two regions are both excited by young massive star clusters containing hundreds of exciting stars and are the largest HII regions in the Local Group. The brightest detected HII region in our study has a luminosity of  $\log(L_{H\alpha}) = 37.8$  before extinction correction which is smaller than the cut offs detected by KEH89 ( $\log(L_{H\alpha}) = 38.6$ ) and WB92 ( $\log(L_{H\alpha}) = 38.2$ ). Their catalogs have problems resolving faint regions especially within crowded spiral arms and at the borders of the brighter HII regions. Our higher detection sensitivity has resolved such regions into smaller ones or individual HII regions (Figure 3). We discuss the resolution effect in more detail in section 4.4.

## 4. Analysis and Discussion

### 4.1. HII Region Luminosity Function in M31

Studying the HII region LF is very important for examining the distribution of massive stars and therefore the star formation in galaxies. The stellar IMF, which is one of the fundamental properties of the star formation process, is believed to be universal as first derived by Salpeter (1955), but new studies suggest a dependence on environmental conditions (e.g. Krumholz & McKee 2008; Meurer et al. 2009). Massive stars are the only

components that can be well-observed in other galaxies to examine the universality of the IMF, although only at the high-mass end (e.g. Calzetti et al. 2010, and references therein). HII region LFs in nearby galaxies have been extensively studied as a characteristic parameter of galaxies (e.g. Kennicutt 1988; Banfi et al. 1993; Rozas et al. 1996; Knapen 1998; Feinstein 1997; Oey & Clarke 1998; Thilker et al. 2000, 2002; Oey et al. 2003; Gutiérrez et al. 2011). Kennicutt (1988) and KEH89 investigated the HII region populations in different types of galaxies and found a large variation along the Hubble sequence. In general, the total number of HII regions increases significantly from Sb galaxies to later Hubble types. The early type galaxies also have a steeper LF and a significant drop in number of very luminous regions with  $L_{H\alpha} > 10^{39}$  erg s $^{-1}$ . Gonzalez Delgado & Perez (1997) studied a sample of spiral galaxies (S0 to Sbc) with active nuclei but they did not find any dependence of the HII LF with Hubble type of the galaxy.

The observed H $\alpha$  emission of HII regions is partially absorbed by dust in the galaxy’s interstellar medium. As a result, the measured flux and luminosity are underestimated, especially toward dense spiral arms. We used the dust optical depth at H $\alpha$  wavelength map made by Tabatabaei & Berkhuijsen (2010) based on the *Spitzer* MIPS data (Gordon et al. 2006) to correct the luminosities. More than 80% of the detected regions were covered in the extinction map. For the remaining 20% we used the uncorrected luminosity but most of these regions are located within the outer disk and are less likely to be affected by dust absorption (Figure 6). The pixel size of the extinction map is 60–70 times larger than that of our images, therefore we matched the position of the peak at each region with the corresponding pixel in the extinction map and used that number to correct the total luminosity of each region as:

$$2.5 \log\left(\frac{L_{corr}}{L_{obs}}\right) = A_{H\alpha} \quad (1)$$

where we have used  $A_{H\alpha} = 1.086\tau_{H\alpha}$  (Caplan & Deharveng 1986).

The primary LF and the final extinction-corrected LF are plotted in Figure 5. We have plotted the LFs derived by KEH89 and WB92 for comparison. The LF is flat in the middle with sharp declines at both bright and faint ends, and is qualitatively similar to those derived in previous works. Turnover points are defined as where the bin counts begin to steadily decrease. KEH89 found that for most galaxies in their sample, the turnover point occurred between  $36 < \log(L_{H\alpha}) < 37$ . However their data (Figure 5) were not deep and resolved enough to find a turnover point for M31. The LF of WB92 shows a flattening between  $\log(L_{H\alpha})=35.2$  and  $36.8$  and a power-law index of  $-1.95$  for  $36.8 < \log(L_{H\alpha}) < 38.2$ . WB92 also suggest a flat theoretical extrapolation for HII LF by KEH98 for  $\log(L_{H\alpha}) < 37$ .

A turnover point in the HII LF is not a characteristic of every galaxy, especially for irregulars (Hodge et al. 1990; Hodge & Lee 1990). Feinstein (1997) predicted that a flat LF

or turnover point could be modelled by considering a constant star formation rate, but a complicated star formation history, such as a burst in the past, would form more faint objects than a constant SFR and make the HII LF complicated. Youngblood & Hunter (1999) found that their sample of 29 normal Im galaxies could be divided into two categories: “Turnover” and “No Turnover”. They argued that the turnover point was not a completeness problem at the low end of the LF, as suggested in some previous works. Galaxies with “Turnover” LFs were found to have a larger number of HII regions, larger luminosity cut-offs, steeper power-law fits and higher SFR per unit area.

Figure 5 clearly shows that the HII region LF in M31 has a faint-end turnover. We are resolving most of the very luminous regions ( $\log(L_{H\alpha}) > 37.5$ ), ionized by multiple stars, into smaller regions and even individual stars. Therefore we adopted a smaller turnover point of  $\log(L_{H\alpha}) = 36.7$ , and the same bin size of 0.2 dex, to be able to compare the results with previous works and to achieve the best fit. The LF was fit using a standard power law:

$$N(L)dL = AL^\alpha dL. \quad (2)$$

We used an average of four 0.2 dex bins with shifts of 0.05 dex in the range  $\log(L_{H\alpha}) = 36.7\text{--}37.8$  to get better statistics and the best correlation coefficient ( $r^2 = 0.96$  and  $\chi^2 = 2.5$ ).

A power-law index of  $\alpha = -2.52 \pm 0.07$  was obtained using least squares fitting and is plotted as the solid black line in Figure 5. This slope is steeper than but consistent with the  $\alpha = -2.3 \pm 0.2$  reported by KEH89 and plotted as the red dotted line in Figure 5. We are resolving most of the luminous regions in the bright end of the KEH89 LF (which refers to multiple ionizing stars), into smaller regions and even individual stars. Therefore a steeper LF, especially at the bright end, is expected. The derived fit, however, is highly dependent on the range of luminosities used.

A double power-law for  $38 < \log(L_{H\alpha}) < 39$ , known as a type II LF, has been reported for individual galaxies in many HII LF studies (e.g. Kennicutt et al. 1989; Rand 1992; Rozas et al. 1996, 1999; Thilker et al. 2000; Gutiérrez et al. 2011). Bradley et al. (2006) used an  $H\alpha$  imaging survey of 53 nearby galaxies (Knapen et al. 2004) to make a composite LF of 17797 HII regions. They found that the LF is steeper for larger luminosities and breaks at a luminosity of  $\log(L_{H\alpha}) = 38.6 \pm 0.1$  with a sharp fall for  $\log(L_{H\alpha}) > 40$ . Pleuss et al. (2000) discussed the resolution effect on determining the HII LF and argued that the type II LF might happen because of the overlapping and blending of smaller HII regions leading to higher measured luminosities. The modelling of HII LFs by Beckman et al. (2000) showed that in case of clustering or overlapping, the LF slope at higher luminosities should decrease, not increase. Instead they suggested that the “glitch” might be caused by the transition of HII regions from ionization bounding at low luminosities (at a critical mass where the

HII region only ionizes its cloud) to density bounding (in which the larger flux of Lyman continuum photons ionizes the diffuse gas and even the intergalactic medium).

The M31 LF upper cutoff is below the type II LF break ( $\log(L_{H\alpha}) = 38.6$ ), which would, in the interpretation of Beckman et al. (2000), imply that all M31 HII regions are ionization bound. However, a large fraction of the total measured  $H\alpha$  luminosity in M31 is emitted by DIG. Giammanco et al. (2004) showed that optically thick clumpy models for HII regions allow a significant fraction of the ionizing photons emitted by the exciting stars to escape from their HII regions. Our observations (e.g. Figure 3) confirm the highly clumped structure of the  $H\alpha$  emission. One of the main reasons that we adopted a larger minimum acceptable size than the image resolution to identify the HII regions was to avoid false detections due to such fluctuations (e.g., see Figure 2).

A large fraction of the detected regions are smaller than the  $\approx 10^{37}$  erg s $^{-1}$  transition point between HII regions ionized by a single star and those ionized by associations and clusters. Therefore a large fraction of detected regions in our study are comparable to typical Galactic HII regions ionized by single OB stars. It is important to note that most of the  $H\alpha$  emission studies in nearby galaxies only probe the massive-star-formation-containing complexes and clusters. HII regions fainter than  $\sim 10^{37}$  erg s $^{-1}$  have not been well studied in external galaxies. They were assumed to generate only a small fraction (5–10%) of the total  $H\alpha$  emission of the galaxies (e.g. KEH89, WB92). M31 is the only exception: KEH89 and WB92 estimated that faint regions contributed at least 30% of the total  $H\alpha$  luminosity. In our survey we have well resolved the major fraction of individual OB stars in associations and field regions below this limit. In total they are responsible for more than 40% of the detected source emission in M31. This result is in contrast with the HII region population and emission in irregular galaxies. Youngblood & Hunter (1999) found that for most of their Im galaxies, 80% of the H II region luminosity is emitted from complexes with typical luminosities of  $10^{37} - 10^{38}$  erg s $^{-1}$ , comparable to 10 Orion nebulae.

Besides the number of faint HII regions in M31, the other notable feature of Figure 5 is that the LF appears to be double-peaked. Our data are complete to  $L_{H\alpha} = 10^{34}$  erg s $^{-1}$ , therefore a second peak at  $10^{35}$  erg s $^{-1}$  suggests a second population of stars. The true location of the second peak may be affected by incompleteness. The first peak at  $10^{35}$  erg s $^{-1}$  and the second peak at  $8 \times 10^{36}$  erg s $^{-1}$  correspond to  $6.6 \times 10^{46}$  and  $5.2 \times 10^{48}$  Lyman- $\alpha$  photons s $^{-1}$  which indicates the emission sources are B0–B1 and O7–O8 stars respectively (Spitzer 1978). The peak at B star luminosities suggest an aged population of massive stars which has lost most of its O stars. The second peak at O stars’ luminosities shows the current massive star formation in M31. It also matches the transition luminosity between HII regions created by individual stars and complexes. The O stars mostly lie in the spiral

arms while the B stars fill the inter-arm regions as well. We discuss the in-arm/inter-arm distribution of the two populations in more detail in section 4.3; however the fact that a fraction of these faint regions are compact and are distributed all over the galaxy disk means that they might be unidentified PNe and not really B stars.

According to Feinstein (1997), a past starburst might be the cause of the first peak at  $L_{H\alpha}=10^{35}$  erg s $^{-1}$ . Comparing the lifetimes of O and B stars ( $\sim 15 \times 10^6$  Myr for an O8 star,  $\sim 20 \times 10^6$  Myr for a B0.5 star) suggests that M31 experienced a star burst between 15 and 20 million years ago. The UV study of the history of star formation in M31 by Kang et al. (2009) also confirms a recent peak in star formation between 10–100 million years ago. The timescale derived here for a recent starburst in M31 is an order of magnitude smaller than the 210 Myr dynamical time derived by Gordon et al. (2006) for the head-on collision between M31 and M32 (Block et al. 2006) that created the 10 kpc star forming ring in M31. McConnachie et al. (2009) detected stars that were remnants of dwarf galaxies destroyed by the tidal field of M31 and suggested that 75% of M31’s dwarf satellites are not yet known. We suggest that the double-peaked LF might also be the result of a more recent collision of M31 with a dwarf satellite galaxy.

#### 4.2. Total $H\alpha$ luminosity and star formation rate

M31’s HII regions are not very luminous compared to giant complexes in other Local Group galaxies. We calculated the total  $H\alpha$  luminosity from M31 HII regions to be  $1.77 \times 10^{40}$  erg s $^{-1}$ , after extinction correction by an average factor of 2.72. This luminosity is comparable with the 30 Doradus complex in the LMC with  $L_{H\alpha} = 1.5 \times 10^{40}$  erg s $^{-1}$  (Kennicutt 1984). It does not include the emission from DIG and PNe. To estimate the contribution to the total galaxy emission from DIG and undetected regions, we measured the total integrated luminosity from each field and subtracted the sum of the HII regions’ luminosities. On average we determined a  $\sim 65\%$  contribution from DIG, PNe and undetected sources. Removed PNe comprise less than 2% of the total luminosity which is even less than the flux measurement uncertainty.

Walterbos & Braun (1994) also reported a large DIG contribution (40%) for M31. Spectrometry studies (Greenawalt et al. 1997b; Galarza et al. 1999) confirmed that the DIG in the disk of M31 is photoionized by a dilute radiation field and there is a smooth transition for line ratios between HII regions and DIG in M31. Thilker et al. (2002) mentioned a leak of ionizing photons from HII regions to the DIG which causes a larger contribution of  $L_{H\alpha}$  by DIG. Beckman et al. (2000) modelled high luminosity HII regions in disk galaxies and showed that regions with  $L_{H\alpha} > 10^{38.6}$  might be density bounded. Such luminous regions emit a

tremendous amount of Lyman continuum photons, sufficient not only to totally ionize the surrounding cloud but also to “leak” into the intergalactic medium. All the HII regions in M31 are smaller than density-bound limit, yet a large fraction of the total  $H\alpha$  emission is contributed by DIG in the disk of the galaxy itself. In another scenario, Giammanco et al. (2004) suggest that the clumpy structure of HII regions may help a large amount of ionizing photons to leak into the surrounding clouds beyond the boundaries of HII regions.

The masked and partially saturated  $10' \times 10'$  bright bulge region also contains a maximum of 10% of the total  $H\alpha$  luminosity. To estimate this contribution we measured the ratio of the total counts in the  $10' \times 10'$  central region to the total counts in the F5- $H\alpha$  field which contained the bulge region. To estimate the total bulge contribution we assumed that every pixel in the  $\sim 2.5' \times 1.5'$  masked bulge in the original image had the limiting saturation value. Then the total luminosity of this field was compared to the total luminosity. Considering that upper limit we calculate a maximum  $H\alpha$  total luminosity of  $5.6 \times 10^{40} \text{ erg s}^{-1}$  for M31. The major uncertainty is caused by the dust attenuation estimation ( $\sim 10\%$ , cf. Tabatabaei & Berkhuijsen 2010) and the DIG estimation (10-15% due to object detection uncertainty in defining DIG). Adding the uncertainty in distance and flux estimation, we have a total uncertainty of 15 – 20% in the total  $H\alpha$  luminosity. Our value is consistent with  $L_{H\alpha} = 4.1 \times 10^{40} \text{ erg s}^{-1}$  [ $4.2 \times 10^{40}$  corrected for distance and using dust attenuation of 2.72 instead of 3.4] determined by Walterbos & Braun (1994)].

Devereux et al. (1994) reported a luminosity of  $(2.8 \pm 0.88) \times 10^{40} \text{ erg s}^{-1}$  [ $(6.2 \pm 1.9) \times 10^{40} \text{ erg s}^{-1}$ , corrected for distance, our own extinction factor and 35% NII contribution]. Their estimation also suffered from background continuum subtraction which led to a 50% flux uncertainty in some filamentary interior regions. Determining the total luminosity is very uncertain due to different assumptions about how to correct the observed flux. For example Barmby et al. (2006) and Tabatabaei & Berkhuijsen (2010) used the raw total  $H\alpha$  luminosity measured by Devereux et al. (1994) and derived two different values of  $9.98 \times 10^{40}$  and  $4.75 \times 10^{40} \text{ erg s}^{-1}$  for corrected  $L_{H\alpha}$ , considering different values for extinction and the [NII] contribution.

We can compare the total  $H\alpha$  luminosity of M31 with other estimates of its overall star formation rate. M31 has been described as a quiescent galaxy with low star formation (Kennicutt 1988). Using the IRAC  $8 \mu\text{m}$  non-stellar luminosity density, Barmby et al. (2006) determined a SFR of  $0.4 \text{ M}_{\odot} \text{ yr}^{-1}$ . We converted the  $H\alpha$  luminosity to SFR using the relation of  $\text{SFR} [\text{M}_{\odot} \text{ yr}^{-1}] = 7.9 \times 10^{-42} L_{H\alpha} [\text{erg s}^{-1}]$  (Kennicutt 1998) and derived a value of  $0.44 \text{ M}_{\odot} \text{ yr}^{-1}$ , close to that of Barmby et al. (2006). Kennicutt et al. (2009) suggested that a combination of IR and  $H\alpha$  gives a better dust-corrected estimation for SFR. We followed

their calibration as:

$$\text{SFR(M)}_{\odot}\text{yr}^{-1} = 7.9 \times 10^{-42} [\text{L}(H\alpha)_{\text{obs}} + 0.020\text{L}(24)] (\text{ergs}^{-1}) \quad (3)$$

where  $\text{L}(H\alpha)_{\text{obs}}$  is the  $H\alpha$  luminosity without correction for internal dust attenuation and  $\text{L}(24)$  is the  $24 \mu\text{m}$  IR luminosity. Adopting  $\text{L}(24) = 1.09 \times 10^{42} \text{ erg s}^{-1}$  from MIPS  $24 \mu\text{m}$  observations (Montalto et al. 2009), the above equation gives a present day SFR of  $0.34 \text{ M}_{\odot} \text{ yr}^{-1}$  which is consistent with the Tabatabaei & Berkhuijsen (2010) range of  $0.27\text{--}0.38 \text{ M}_{\odot} \text{ yr}^{-1}$ . A comparison of different M31 SFRs from previous studies is summarized in Table 4. They cover a wide range from  $0.27$  to  $1 \text{ M}_{\odot} \text{ yr}^{-1}$ . In a UV study on star forming regions in M31, Kang et al. (2009) argued that M31 has no FUV-detected massive star forming regions younger than 50 Myr. Those authors concluded that the SFR in M31 is decreasing from a possible peak between  $\sim 10$  and  $100$  Myr ago.

### 4.3. Comparison of In-arm and Inter-arm Regions

Statistical studies of HII regions often show differences in properties between sources located in galaxies’ spiral arms or in the gaps between the arms (e.g. Rand 1992; Thilker et al. 2000; Scoville et al. 2001). For example, Figure 1 shows that the bright sources in M31 are generally located only in the arms and noticeably trace the  $10 \text{ kpc}$  star forming ring while the fainter sources are scattered between the arms as well. Banfi et al. (1993) reported a morphology dependence of the HII LF and also different HII LFs for in-arm and inter-arm regions in a sample of Virgo cluster galaxies. Rand (1992) and Thilker et al. (2000) also found different LF slopes for in-arm and inter-arm regions but the difference was not significant. Different LFs for in-arm/inter-arm regions have not been observed in many other spiral galaxies (e.g. Knapen 1998; Rozas et al. 1996; Gutiérrez et al. 2011). The presence of larger HII regions within spiral arms might be only a statistical effect, not a physical difference between in-arm and inter-arm regions: spiral arms contain more HII regions and therefore also more luminous regions (Knapen 1998).

Oey & Clarke (1998) used Monte Carlo simulations to study the evolution of LFs and suggested that the arm populations represent the currently active star forming regions while the inter-arm regions are aged populations. However, those authors noted that the timescale of passing between spiral density waves at any location within the disk is about  $40 \text{ Myr}$  which is much larger than the maximum observable  $24 \text{ Myr}$  lifetime of the HII regions (Oey et al. 2003). Therefore a fraction of new stars must be born in inter-arm regions as well.

The spiral arms in M31 are identified by highly concentrated gas and dust. Tabatabaei & Berkhuijsen (2010) showed a good correlation between the  $H\alpha$  and  $70 \mu\text{m}$  emission; therefore the distri-



bution of the dust optical depth at  $H\alpha$  wavelength is an appropriate mask to select in-arm and inter-arm HII regions. We used the Tabatabaei & Berkhuijsen (2010)  $\tau_{H\alpha}$  to designate the arm HII regions. All the sources with extinction  $> 0.7$  were assigned to the arm population. Figure 7 shows the in-arm and inter-arm LFs using the dust distribution masking. The solid line and dashed lines present in-arm and inter-arm regions respectively. The straight lines are the power law fits. The in-arm regions are best fitted with a power-law with  $\alpha = -2.43 \pm 0.22$  and inter-arm regions with  $\alpha = -2.40 \pm 0.22$ . The inter-arm regions are less luminous and less populated and comprise only 40% of the total detected regions and 14% of the total detected emission. The brightest inter-arm region has a luminosity of  $L_{H\alpha} = 2.80 \times 10^{37} \text{ erg s}^{-1}$ , nearly 10 times fainter than the most luminous object with  $L_{H\alpha} = 2.21 \times 10^{38} \text{ erg s}^{-1}$ .

Knapen (1998) suggested that the lack of bright HII regions in inter-arm regions is only a statistical effect and that the same LF slope for in-arm and inter-arm regions confirms that both have the same population. However their data were not deep enough to detect individual faint HII regions created by aged B stars. Figure 7 clearly shows two different populations for in-arm and inter-arm regions in M31. The in-arm LF peaks at brighter regions and presents current star formation. The inter-arm LF peaks at aged B stars, as suggested by Oey & Clarke (1998) and Oey et al. (2003). If we accept that inter-arm regions have the same population as in-arm regions but scaled to smaller numbers, then we also expect fewer HII regions in lower luminosity bins. Surprisingly, the number of HII regions created by B stars between the arms is noticeably larger than the in-arm regions within the same luminosity bin. As discussed before the dynamical travel time between spiral density waves ( $\sim 40 \text{ Myr}$ ) is larger than the evolution time of HII regions ( $\sim 24 \text{ Myr}$ ). Therefore to explain the extraordinary large number of faint HII regions between M31’s spiral arms we should either assume that a large number of massive stars are formed in inter-arm regions (which is not probable because there is not enough gas to form too many massive stars) or accept that the SFR has been larger in the past. The noticeable fraction of B stars in the inter-arm regions therefore supports the hypothesis of a recent star burst in M31.

#### 4.4. Size Distribution of HII Regions in M31

In contrast to the Milky Way, LMC, or many spiral galaxies such as M51 and M33, M31 does not have very luminous HII regions. Here we examine whether this is due to higher resolution in M31, resolving larger regions into smaller ones, or an intrinsic lack of giant HII regions in M31.

Scoville et al. (2001) studied the HII regions in M51 with high angular resolution ( $0.1''$ – $0.2''$ , 4.6–9.3 pc) *HST* imaging. With spatial resolution similar to this work, they detected HII regions between 10–250 pc with  $L_{H\alpha} \approx 2 \times 10^{36} - 2 \times 10^{39} \text{ erg s}^{-1}$ . Gutiérrez et al. (2011) made a similar *HST* survey of M51 and found a size range of 8.3–530 pc. They found two populations which are separated at  $D \simeq 120$  pc and suggested that size as a transition between HII regions ionized by a single OB cluster and multiple regions.

Both groups defined the effective size based on the area covered by the region rather than the FWHM as used in this work. The FWHM size is slightly smaller especially in diffuse regions but the size range of M31’s HII regions ( $\sim 16 - 190$  pc) is still comparable with M51 and the Galactic HII regions. Despite the similarity in size, M31 does not have very luminous HII regions like M51 or the most luminous Galactic HII regions such as W49 ( $L_{H\alpha} = 9.1 \times 10^{38} \text{ erg s}^{-1}$ ) and W51 ( $L_{H\alpha} = 3.9 \times 10^{38} \text{ erg s}^{-1}$ ; Schraml & Mezger 1969). A similar *HST* study by Pleuss et al. (2000) on M101’s HII regions showed the same range of size (10–220 pc) and luminosity ( $\sim 10^{36} - 2 \times 10^{39} \text{ erg s}^{-1}$ ).

Assuming a lifetime of  $3 \times 10^6$  yr for the OB stars to produce most of the ionizing photons, Scoville et al. (2001) considered an upper limit of 50 pc for the radius of HII regions created by a single OB star cluster. They concluded a maximum luminosity of  $L_{H\alpha} \sim 10^{39} \text{ erg s}^{-1}$  for a single cluster and reported any larger or brighter region as a blend of multiple regions. All the regions in our catalog have smaller luminosities than this upper limit, but there are some regions extended to radii larger than 50 pc. HII regions grow very fast in their early phase until they reach the Strömgren radius. The ionization front may expand to the diffuse ionized gas after a steady hydrodynamic growth beyond the Strömgren sphere. Extended HII regions in M31 are most probably evolved regions which are not as luminous as when they formed. They might look extended due to the leakage of the ionizing UV photons as well. The lack of giant HII regions in M31 remains as yet unexplained.

The power law LF of HII regions is well accepted for all different types of galaxies, although the slope apparently depends on galaxy type and may vary for different galaxy components. One then expects to observe a power-law size distribution as well, because the luminosity depends on the volume and therefore the size of the HII region (van den Bergh 1981; Oey et al. 2003). Assuming  $L \propto D^3$  and  $dL/dD \propto D^2$ , the differential size distribution should be (Oey et al. 2003):

$$N(D)dD = N(L)\frac{dL}{dD} \propto D^{2+3\alpha}dD. \quad (4)$$

Therefore the luminosity and size distribution slopes should be related as  $\beta = 2 + 3\alpha$ .

The edges which HIIphot uses to determine the total flux of each source are based on the background emission. For individual spherical HII regions the  $\text{FWHM}_{\text{eff}}$  is close to half

of the assigned border diameter, but in crowded regions especially with strong background DIG, the assigned borders are much larger than the  $\text{FWHM}_{\text{eff}}$ . The fact that in some regions the reported flux has been integrated on a larger area than the defined effective size may affect the relation between LF and size distribution. We fit a power law size distribution:

$$N(D) \propto D^{\beta} dD \quad (5)$$

where  $D$  is the effective FWHM size of the region multiplied by two.

Figure 8 shows the HII regions’ diameter distribution. Similar to Gutiérrez et al. (2011) we also see a sharp fall for regions larger than 130 pc (the transition between single OB star regions and blends of multiple regions). The dashed line presents the best fit for all the regions smaller than 130 pc and the dotted line presents the fit for  $D > 130$  pc. We derived a slope of  $-3.3 \pm 0.11$  for the distribution of the smaller regions and  $-5.40 \pm 0.24$  for the larger end ( $D > 130$  pc) of the size distribution. Due to the galaxy’s proximity, most of the larger regions in M31 are resolved, therefore we consider only the large end of the size distribution for comparison with other galaxies. Values between  $-3.33$  and  $-5.50$  have been observed for regions with  $\log(D/\text{pc}) \geq 2.3$  for a range of Hubble types from Sb to Sm-IV (Figure 2 in Oey et al. 2003), so M31 is consistent with the general trend. Using Eq. 4 and our value for  $\alpha = -2.4 \pm 0.17$ , we predict  $\beta = -5.2 \pm 0.51$  which is consistent with our fit to the size distribution. The agreement seems surprisingly good, given that the size that HIIphot uses to measure the total flux of a region is not the same as the effective size (FWHM of the luminosity peak); however, if most of the luminosity of a region is in the central peak rather than the faint outskirts then the agreement is understandable.

#### 4.5. Comparison of HII Regions to Young Clusters in M31

It is well accepted that the star formation rate is correlated with the amount of gas in star forming regions and the gas surface density (e.g. Kennicutt 1998). Most of the molecular gas lies in spiral arms in a galaxy, therefore it is expected that the major fraction of the star formation takes place in spiral arms. Most of the stars, and particularly massive stars, form within clusters and create HII regions by ionizing the surrounding gas. In this section we study the correlation between HII regions and stellar clusters in M31. We used the Caldwell catalog (Caldwell et al. 2009) and the HST/WFPC survey of bright young clusters in M31 (Krienke & Hodge 2007; Hodge et al. 2009, 2010; Perina et al. 2010) to examine the spatial correlation of HII regions with young stellar clusters.

The Caldwell et al. (2009) catalog contains 670 clusters of different types, 140 of which are identified as young clusters. The HST survey (referred to below as the ‘KH catalog’) and

its follow-ups contains 714 clusters, including 67 previously known objects and 24 clusters in common with Caldwell. Only 7 young clusters (age < 2 Gyr) from the Caldwell catalog were matched within a  $10''$  ( $\sim 38$  pc) neighbourhood (typical size of the Caldwell clusters). The age of the Caldwell clusters ( $\sim 2$  Gyr) is much larger than the few Myr lifetime of the HII regions so the lack of matches was not a surprise. In contrast, we found an additional 43 HII regions matched with the KH list within a  $4''$  neighbourhood (the typical size of the new KH clusters and the minimum size of our HII regions). Krienke & Hodge (2007) used only 39 HST pointings which cover a very small fraction of the entire disk. By extrapolating the data they estimated that the entire disk may contain  $\approx 80000$  stellar clusters. Following their estimation we expect 4370 matches between HII regions and clusters. This number is larger than our total number of HII regions; however we already have regions within the KH fields which are not matched with clusters. Overall, we find a reasonable correlation between the location of HII regions and clusters.

Figure 9 compares the locations of the detected HII regions and matched clusters. Grey and cyan dots present the location of faint and luminous HII regions. Interestingly, the clusters matched with HII regions also lie within the spiral arms, indicating that the clusters within the arms still contain multiple massive stars which can create very luminous HII regions. As discussed above, the luminous HII regions trace the spiral structure and 10 kpc star forming ring. The fainter regions are scattered within the arms as well and are more concentrated toward the center (also shown in Figure 1). We removed all the known and potential PNe from our catalog, but some of these faint central regions, especially the compact ones, might be unidentified PNe. The expected lack of active star formation in this gas-poor part of the galaxy is a further argument for some of these objects being PNe associated with the old stellar population of the bulge.

Schruba et al. (2010) recently showed that the Kennicutt-Schmidt law (power law dependence of star formation rate on molecular gas surface density; Kennicutt 1998) which is observed and well accepted for kpc scales breaks down on smaller scales (e.g. aperture size of  $\lesssim 300$  pc for M33). They concluded that individual GMCs present a range of evolutionary states in their 20 – 30 Myr lifetime which could be studied by recent ( $H\alpha$ ) and future (CO) star formation tracers. If we extend these results into our observations of recent star formation as detected in HII regions in highly extincted regions, we may conclude that some very young clusters are missing in this study. Presumably such clusters are deeply embedded in molecular clouds and would be more easily detected at infrared wavelengths, such as with the *Herschel Space Observatory* or James Webb Space Telescope.

## 5. Summary and Conclusion

We used the data from the Survey of Local Group Galaxies (Massey et al. 2006) to construct a complete catalog of HII regions in M31. The results of this work are summarized below:

1. Using H $\alpha$  and R band images of M31, we applied the HIIphot code in order to catalog the HII regions of the galaxy. The catalog contains 3961 regions to a limiting flux of  $\sim 10^{-16}$  erg cm $^{-2}$  s $^{-1}$  after removing matched planetary nebulae and potential PNe. The luminosity derived for each region was corrected for extinction using *Spitzer* MIPS dust maps. Detected regions with  $L_{H\alpha} \geq 10^{36}$  erg s $^{-1}$  clearly trace the spiral structure of the galaxy while fainter regions scatter through the disk with an increasing number density toward the center. The most luminous region in our catalog, with  $L_{H\alpha} = 2.2 \times 10^{38}$  erg s $^{-1}$ , confirms that M31 does not have giant HII regions such as those in the Milky Way, LMC, M33 and M51.
2. We measured a total H $\alpha$  luminosity of  $5.6 \times 10^{40}$  erg s $^{-1}$  which contains a 65% contribution from diffuse ionized gas and has about 20% uncertainty. Despite the general belief that small individual HII regions only supply a small fraction of the total H $\alpha$  emission in most galaxies, 60% of the total  $L_{H\alpha}$  from HII regions in M31 is contributed by regions with  $L_{H\alpha} < 10^{37}$  erg s $^{-1}$ . This large fraction also contains the regions at peripheries of larger complexes that have not been resolved in other studies. In total we determined a SFR=0.44 M $_{\odot}$  yr $^{-1}$ , in agreement with Barmby et al. (2006) (0.4 M $_{\odot}$  yr $^{-1}$ ).
3. The luminosity function ( $N(L)dL = AL^{\alpha}dL$ ) and size distribution ( $N(D)dD = AD^{\beta}dD$ ) obtained from the catalog are reasonably fitted by power law distributions. A slope of  $\alpha = -2.52 \pm 0.07$  was obtained for the LF, which is consistent with  $-2.3 \pm 0.2$  determined by Kennicutt et al. (1989). We detect a break in the size distribution function at  $\sim 130$  pc, close to 120 pc which is suggested to be the transition between HII regions ionized by a single OB cluster to multiple regions in M51 (Gutiérrez et al. 2011). The power law fit to the size distribution for diameters smaller than 130 pc yields a slope of  $-3.23 \pm 0.11$  and a slope of  $-5.40 \pm 0.24$  for  $D > 130$  pc, within the range of the typical distribution for spiral galaxies but steeper than most Sb galaxies (Oey et al. 2003).
4. The luminosity function has two distinct peaks at approximate  $L_{H\alpha} = 10^{35}$  and  $4 \times 10^{36}$  erg s $^{-1}$ . The peak at fainter luminosities is from the population of inter-arm regions and might be contaminated by unidentified PNe. The second peak luminosity, which

also matches with B stars, suggests a starburst 15–20 Myr ago. This timescale is consistent with the results of UV studies which suggest a starburst sometime between 10 and 100 Myr ago.

5. Massive stars form in stellar clusters, therefore we examined the correlation between the HII regions and star clusters. The clusters which spatially match with HII regions approximately lie within the arms. Considering the incompleteness of the M31 young cluster catalogs, we found a good statistical match between the location of HII regions and clusters.

We thank Fatemeh Tabatabaei for providing the extinction map for M31 and Johan Knapen for useful comments and suggestions on a draft of the paper. Nelson Caldwell and Philip Massey are thanked for helpful discussions and suggestions. We also thank the anonymous referee for detailed comments and suggestions that helped to improve this work. Support for this research was provided by a Discovery Grant from the Natural Sciences and Engineering Research Council of Canada and an Ontario Early Researcher Award, both to PB.

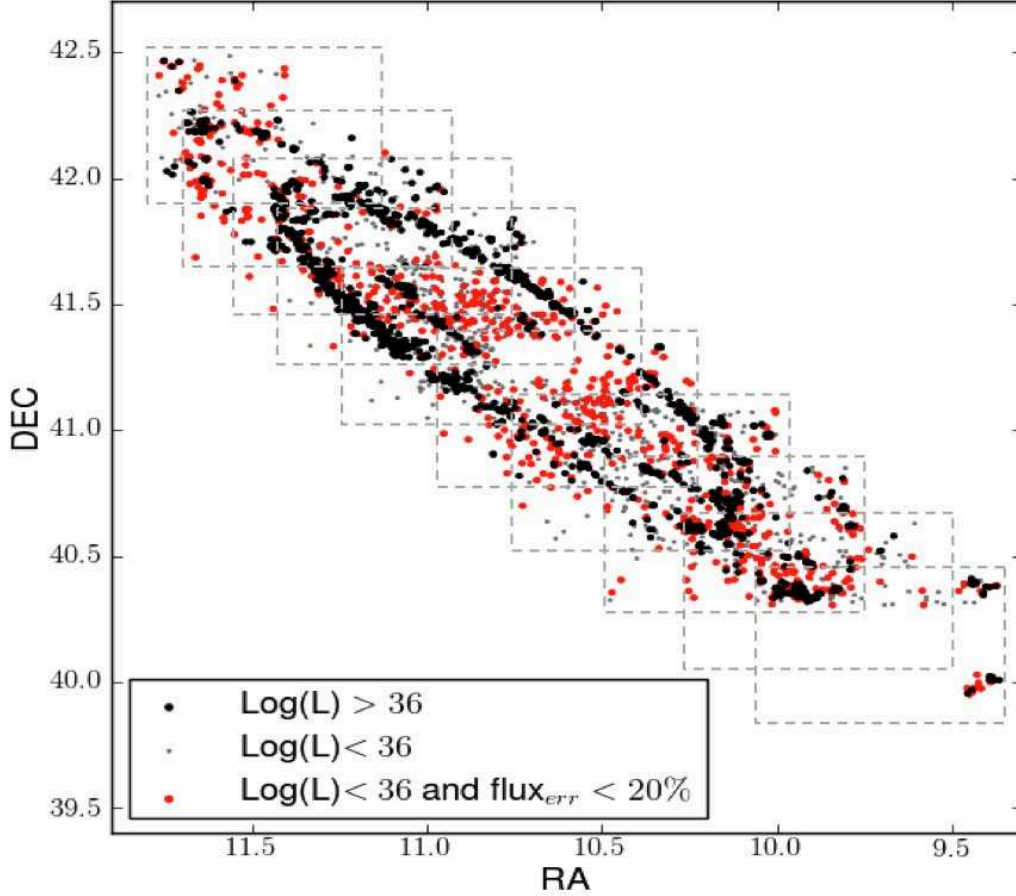


Fig. 1.— Coordinate plot of HII regions in M31, with north up and east left. Dashed rectangles show the 10 fields observed by Massey et al. (2006) numbered from top to bottom. The black dots indicate the regions with  $H\alpha$  luminosities  $\geq 10^{36} \text{ erg s}^{-1}$ . Grey dots are regions with luminosities  $L_{H\alpha} < 10^{36} \text{ erg s}^{-1}$  and red dots present the same regions with a final flux uncertainty less than 20%. The central bulge is masked with a  $10' \times 10'$  box. The higher luminosity regions clearly trace the spiral arms while the lower luminosity regions also fill up the inter-arm spaces with a concentration toward the center.

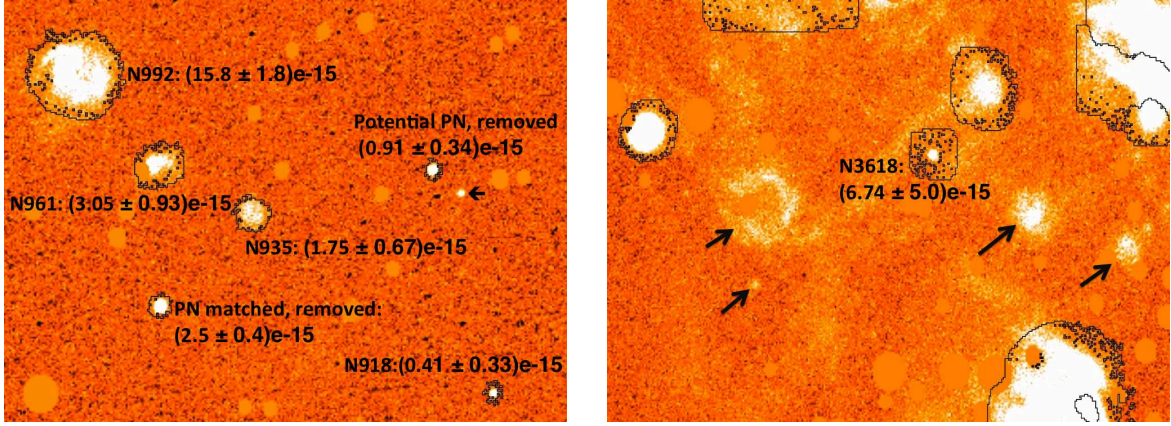


Fig. 2.— Example of HII region detection. The solid circles are removed stars. All the regions have an initial S/N detection of 10 or larger, however the final flux uncertainty is relatively large due to the background emission. The numbers following the source catalog number on each image show the flux and its uncertainty. Two of the detected regions in the left panel were matched with PNe lists and removed. The right panel shows region N3618 which lies within a filament. The source is a compact bright object but due to the DIG background emission, it has a large uncertainty in flux determination. There are four other regions marked by arrows which did not pass the high S/N=10 detection limit. The emission of these regions has been included as part of the DIG in computing the total H $\alpha$  emission of the galaxy.



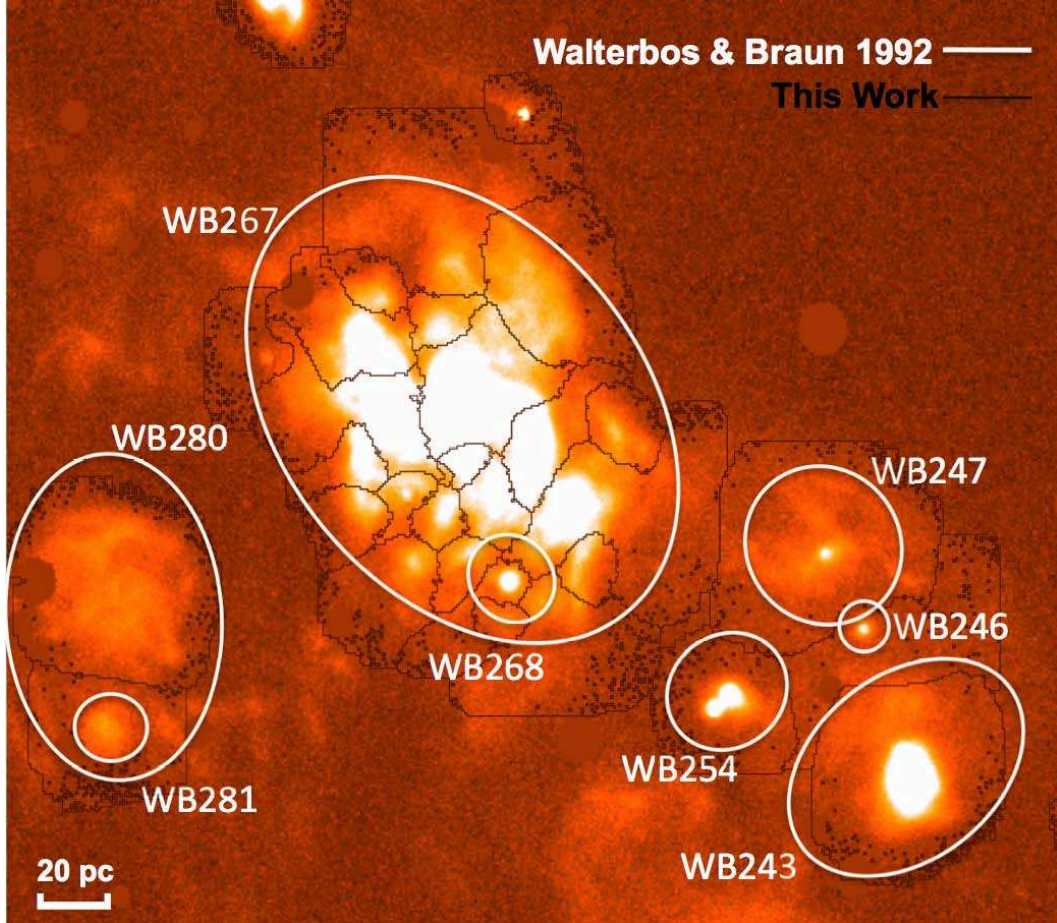


Fig. 3.— A sample comparison between our catalog and WB92. Black lines show the borders determined by HIIphot and white ellipses show the same regions in WB92 (a color version of this figure is available in the online edition).

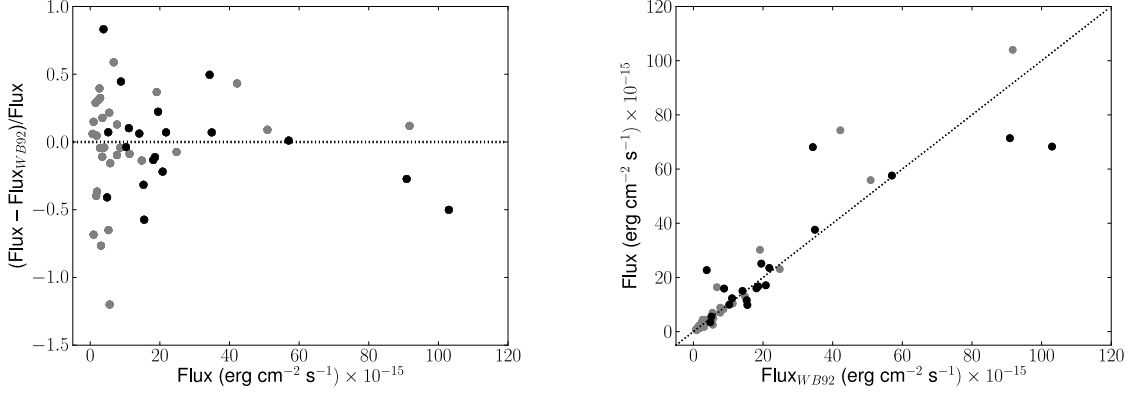


Fig. 4.— Comparison between flux measurements in Walterbos & Braun (1992) and this work. The grey show all the matched regions with a separation  $\leq 0.5''$  and black dots present only larger ( $\geq 12$  pixels, 11.75 pc) well-resolved regions.

Table 1. Scaling factors for H $\alpha$  continuum subtraction of Local Group Survey M31 images

Field	Scaling factor
1	0.378
2	0.855
3	0.379
4	0.395
5	0.363
6	0.393
7	0.386
8	0.418
9	0.400
10	0.396

Note. — Scaling factors are the average ratio of H $\alpha$  to  $R$ -band total flux (as measured in the original image units) of bright stars in each field. See text for discussion of field 2.

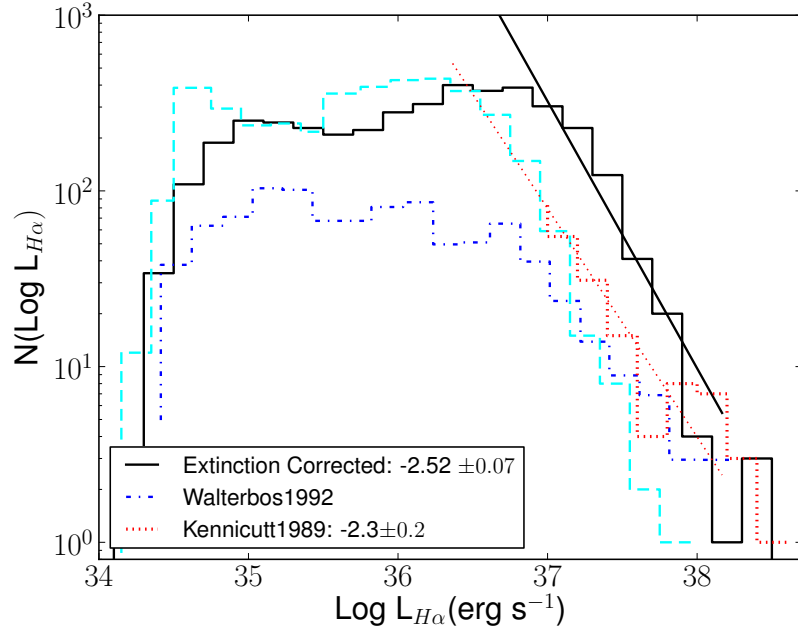


Fig. 5.— M31 HII region luminosity function, after removing the planetary nebulae. The dashed cyan and solid black histograms show the LF before and after correction for extinction. The solid black line shows the least squares fit with slope of  $\alpha = -2.52 \pm 0.07$  using an average of four different 0.2 dex bins within  $\log(L_{H\alpha}) = 36.70 - 37.80$  each shifted 0.05 dex. For comparison the KEH89 and the WB92 results are plotted in red dotted and blue dash-dotted lines respectively. The dotted red straight line shows the KEH89 power law with  $\alpha = -2.3 \pm 0.2$  [note that the fitted slope for  $\log N(\log L_{H\alpha})$  versus  $\log(L_{H\alpha})$  is  $1 - \alpha$ ]. Two distinct peaks at luminosities corresponding to B0 and O7–O9 stars are noticeable.

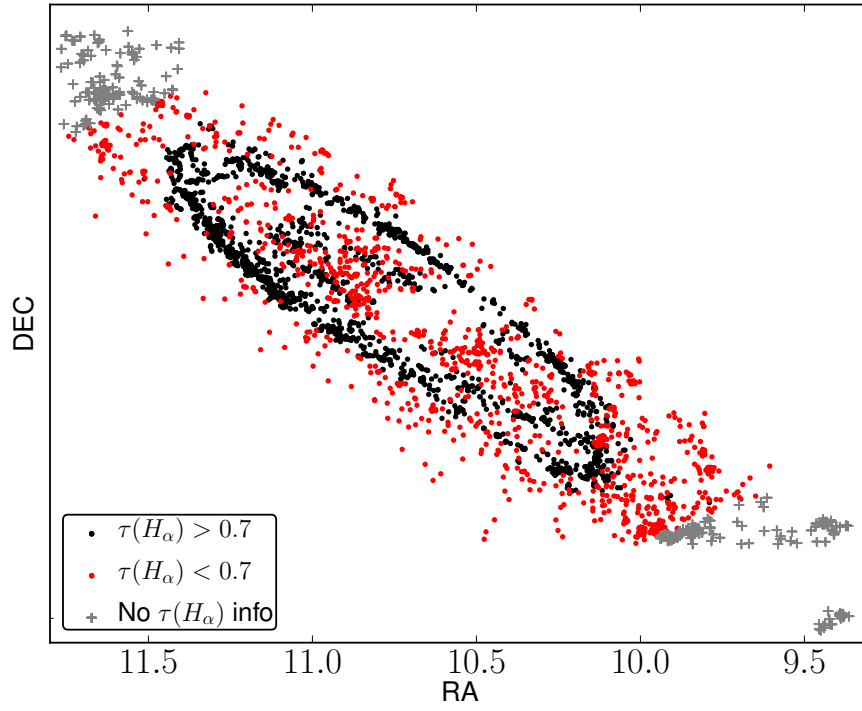


Fig. 6.— In-arm and inter-arm regions selected based on the spiral arm structure in dust. Black and red dots present regions with  $\tau(H\alpha) > 0.7$  and  $\tau(H\alpha) < 0.7$  respectively. Grey crosses are regions for which we do not have the extinction information, but based on their location at the edges of the disk, we have considered them as inter-arm regions.

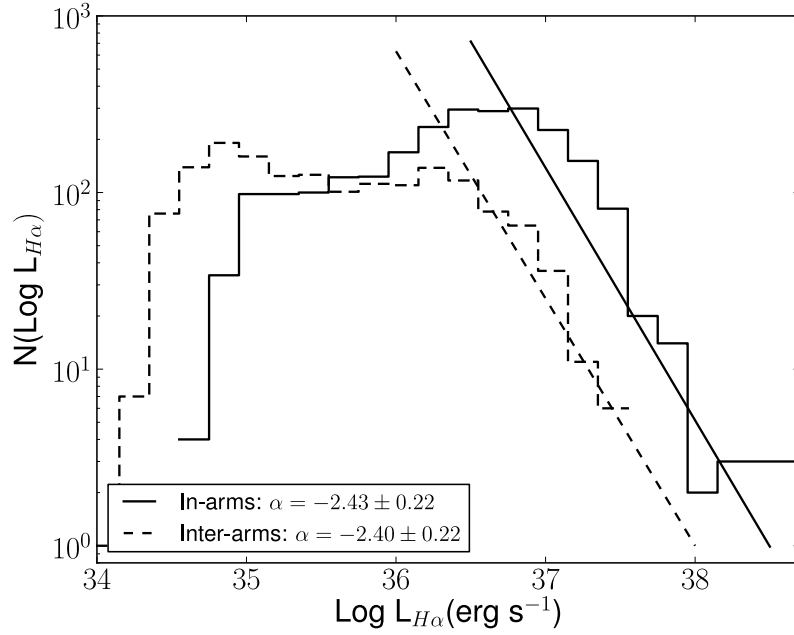


Fig. 7.— The in-arm/inter-arm luminosity functions selected by  $H\alpha$  optical depth. It is noticeable that brighter regions lie within the arms while fainter regions cover the inter-arms. The spiral arms contain most of the young newborn stars and, similar to the total, their LF peaks at O6-O7 stars. As suggested by Oey & Clarke (1998) the aged stars may leave the original cloud in which they form and fill up the gaps between the arms. There is no significant difference in the power law slopes for the two categories.

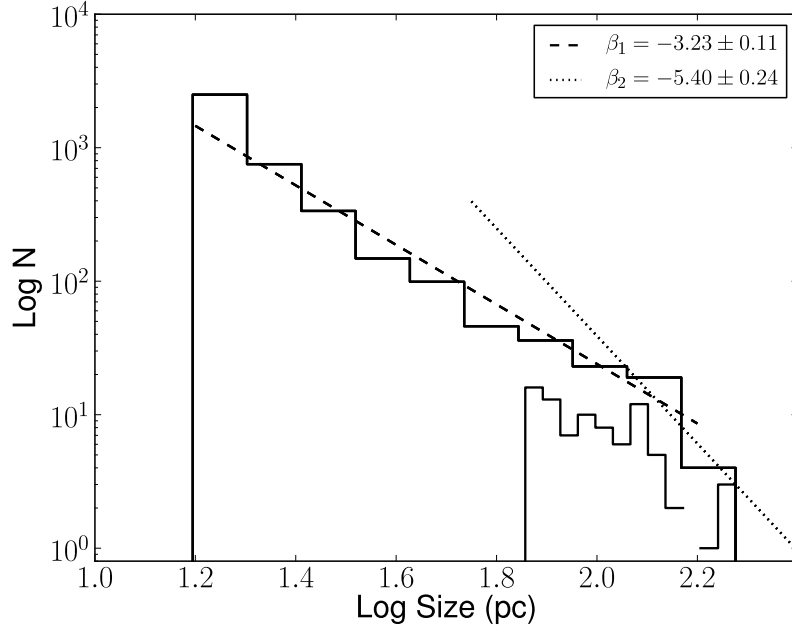


Fig. 8.— Size distribution of the HII regions. The right corner histogram shows only larger regions ( $\log(D[\text{pc}]) > 1.84$ ) with 1/3 smaller bins. The dashed line presents the best power law fit for  $D < 130$  pc and dotted line presents the larger end ( $D \geq 130$  pc) [note that the fitted slope for  $\log N(\log D)$  vs.  $\log(D)$  is  $1 - \beta$ ].

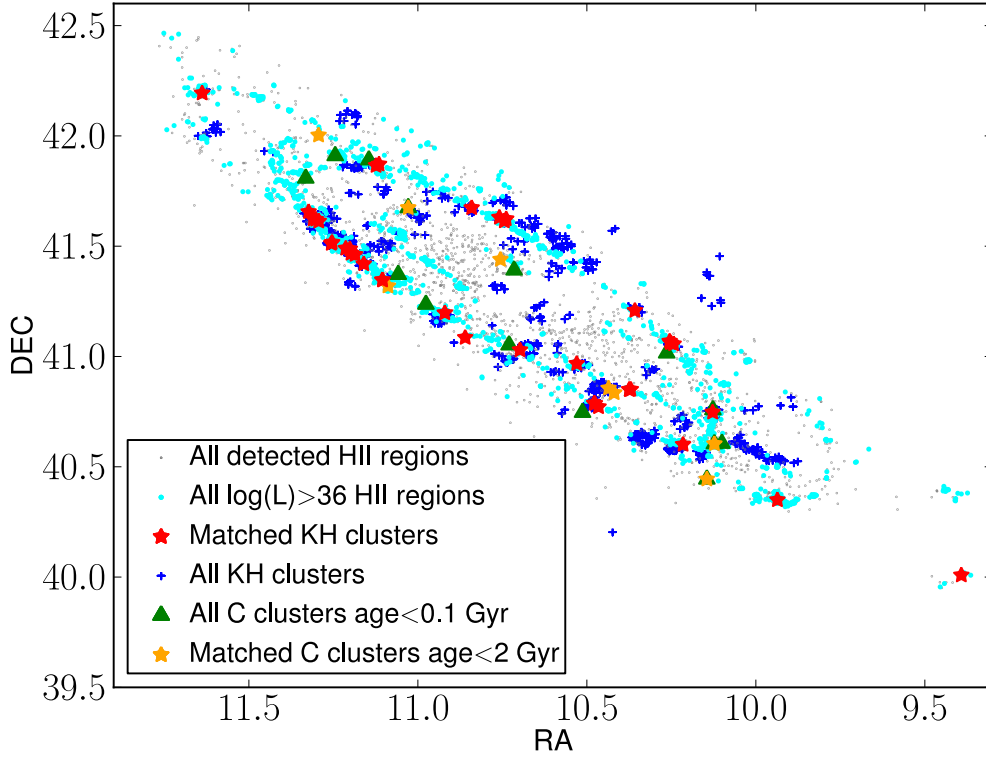


Fig. 9.— An overlay of HII regions and star clusters in M31. The HII regions with  $L_{H\alpha} \geq 10^{36}$  erg s $^{-1}$  are shown in cyan and other regions in grey dots. The blue crosses represent all the KH clusters. Green triangles present all the Caldwell young clusters (age  $< 0.1$  Gyr). Red and orange stars present the matched HII regions with the KH and Caldwell (age  $< 2$  Gyr only) clusters respectively. As expected most of the matches lie in spiral arms.

Table 2. Catalog of HII regions in M31

ID	Field	RA <sub>(J2000)</sub> (deg)	DEC <sub>(J2000)</sub> (deg)	FWHM <sub>maj</sub> ( $''$ )	FWHM <sub>min</sub> ( $''$ )	PA (deg)	D (pc)	Flux ( $\times 10^{-15}$ ) (erg cm $^{-2}$ s $^{-1}$ )	Extinction (mag)	Luminosity <sub>cor</sub> $\times 10^{34}$ (erg s $^{-1}$ )
904	F9	10.2175	40.5493	4.65	2.66	105	26.67	19.50 $\pm$ 1.67	1.341	492
905	F7	10.2175	40.6027	3.64	2.08	135	20.85	7.32 $\pm$ 1.93	0.892	122
906	F7	10.2175	40.6224	2.78	1.85	75	17.23	4.63 $\pm$ 2.38	2.396	309
907	F9	10.2179	40.5306	2.79	2.23	90	18.95	1.78 $\pm$ 0.71	0.664	23.9
908	F8	10.2183	40.548	18.04	14.43	120	122.43	68.20 $\pm$ 1.69	1.341	1720
909	F8	10.2183	40.6016	3.21	1.61	0	17.23	16.50 $\pm$ 0.19	0.771	246
910	F8	10.2187	40.5547	2.54	2.03	90	17.23	0.76 $\pm$ 0.36	1.265	17.8
911	F7	10.2196	41.0024	4.66	4.66	0	35.40	3.17 $\pm$ 0.90	1.072	62.3
912	F8	10.2204	40.5397	4.27	2.14	60	22.93	19.90 $\pm$ 0.91	1.018	374
913	F9	10.2204	40.5473	3.53	1.77	165	18.95	6.39 $\pm$ 0.99	1.227	145
914	F8	10.2208	40.5383	2.79	2.23	45	18.95	60.30 $\pm$ 1.04	0.914	103
915	F8	10.2208	40.7258	2.27	2.27	0	17.23	4.20 $\pm$ 0.86	1.239	96.4
916	F7	10.2212	40.9862	3.89	1.94	45	20.85	9.03 $\pm$ 1.38	0.952	159
917	F7	10.2212	41.0138	2.31	1.85	0	15.66	0.41 $\pm$ 0.33	1.499	12.0
918	F9	10.2217	40.5484	5.45	2.73	165	29.25	3.65 $\pm$ 0.85	1.227	82.8
919	F8	10.2229	40.5375	2.78	1.85	60	17.23	1.75 $\pm$ 0.34	0.914	29.9
920	F8	10.2246	40.6179	4.84	2.76	135	27.74	13.30 $\pm$ 0.22	2.409	899
921	F8	10.2263	40.6409	2.27	2.27	0	17.23	0.52 $\pm$ 0.04	1.244	11.9
922	F7	10.2263	40.7661	5.85	3.34	105	33.58	10.90 $\pm$ 2.90	1.149	231
923	F8	10.2271	40.6194	2.54	2.03	90	17.23	6.46 $\pm$ 0.17	2.637	537



Table 3. Catalog of potential PNe, removed from final HII region catalog

ID	Field	RA <sub>(J2000)</sub> (deg)	DEC <sub>(J2000)</sub> (deg)	FWHM <sub>maj</sub> ( $''$ )	FWHM <sub>min</sub> ( $''$ )	PA (deg)	D (pc)	Flux ( $\times 10^{-15}$ ) (erg cm $^{-2}$ s $^{-1}$ )	Extinction (mag)	Luminosity <sub>cor</sub> $\times 10^{34}$ (erg s $^{-1}$ )	Merrett et al. (2006) Catalog number
100	F8	10.2196	40.6769	2.538	2.031	45	17.230	0.671 $\pm$ 0.0387	0.503	7.81	2918
101	F7	10.2242	41.023	2.308	1.846	0	15.664	0.909 $\pm$ 0.344	1.368	23.5	1550
102	F8	10.2263	40.5382	2.308	1.846	0	15.664	0.743 $\pm$ 0.259	0.839	11.8	2264
103	F6	10.2263	41.1441	2.064	2.064	0	15.664	2.1 $\pm$ 0.161	0.000	15.4	3041
104	F8	10.2317	40.7221	2.538	2.031	135	17.230	0.549 $\pm$ 0.24	1.043	10.5	1907
105	F7	10.235	40.8982	2.064	2.064	0	15.664	2.49 $\pm$ 0.169	0.390	26.2	1778
106	F7	10.2358	40.7829	2.064	2.064	0	15.664	3.55 $\pm$ 0.904	1.048	68.4	1923
107	F7	10.245	40.8629	2.308	1.846	0	15.664	0.977 $\pm$ 0.238	0.632	12.8	1772
108	F7	10.2471	41.0494	2.308	1.846	0	15.664	2.95 $\pm$ 0.486	1.438	81.5	1556
109	F8	10.2513	40.4805	2.064	2.064	0	15.664	1.86 $\pm$ 0.256	0.000	13.6	2256
110	F7	10.2513	40.8982	2.918	1.460	105	15.664	0.543 $\pm$ 0.149	0.429	5.91	2877
111	F7	10.2613	41.1157	2.064	2.064	0	15.664	1.22 $\pm$ 0.347	0.874	19.9	1570
112	F8	10.2742	40.4704	2.538	2.031	120	17.230	0.568 $\pm$ 0.188	0.000	4.16	2251
113	F7	10.2808	40.843	2.064	2.064	0	15.664	1.98 $\pm$ 1.21	0.627	25.9	2876
114	F6	10.3058	41.193	2.064	2.064	0	15.664	0.722 $\pm$ 0.153	0.847	11.5	1033
115	F7	10.3083	40.7816	2.064	2.064	0	15.664	2.76 $\pm$ 1.41	0.594	35	1922
116	F7	10.3112	40.7425	2.064	2.064	0	15.664	5.63 $\pm$ 3.22	0.000	41.3	1910
117	F6	10.3217	41.2672	2.064	2.064	0	15.664	1.22 $\pm$ 0.104	0.546	14.7	1053
118	F6	10.3229	41.2018	2.064	2.064	0	15.664	1.56 $\pm$ 0.158	0.969	27.9	1039
119	F7	10.3233	40.9791	2.064	2.064	0	15.664	2.06 $\pm$ 0.592	0.546	24.9	1760
120	F6	10.3363	41.1714	2.064	2.064	0	15.664	1.76 $\pm$ 0.11	1.382	45.9	1029

Table 4. Star formation rates for M31

Data	Method	SFR ( $M_{\odot} \text{ yr}^{-1}$ )
Tabatabaei & Berkhuijsen (2010)	extinction corrected $H_{\alpha}$	0.27–0.38
Kang et al. (2009)	UV SF regions, 400 Myr avg	0.6–0.7
Barmby et al. (2006)	Infrared $8\mu\text{m}$ Luminosity	0.4
Williams (2003)	Optical photometry	$\sim 1$
Walterbos & Braun (1994)	extinction corrected $H_{\alpha}$	0.35

## REFERENCES

- Arp, H. 1973, *ApJ*, 185, 797
- Baade, W. & Arp, H. 1964, *ApJ*, 139, 1027
- Banfi, M., Rampazzo, R., Chincarini, G., & Henry, R. B. C. 1993, *A&A*, 280, 373
- Barmby, P., Ashby, M. L. N., Bianchi, L., Engelbracht, C. W., Gehrz, R. D., Gordon, K. D., Hinz, J. L., Huchra, J. P., Humphreys, R. M., Pahre, M. A., Pérez-González, P. G., Polonski, E. F., Rieke, G. H., Thilker, D. A., Willner, S. P., & Woodward, C. E. 2006, *ApJ*, 650, L45
- Beckman, J. E., Rozas, M., Zurita, A., Watson, R. A., & Knapen, J. H. 2000, *AJ*, 119, 2728
- Block, D. L., Bournaud, F., Combes, F., Groess, R., Barmby, P., Ashby, M. L. N., Fazio, G. G., Pahre, M. A., & Willner, S. P. 2006, *Nature*, 443, 832
- Bradley, T. R., Knapen, J. H., Beckman, J. E., & Folkes, S. L. 2006, *A&A*, 459, L13
- Caldwell, N., Harding, P., Morrison, H., Rose, J. A., Schiavon, R., & Kriessler, J. 2009, *AJ*, 137, 94
- Calzetti, D., Chandar, R., Lee, J. C., Elmegreen, B. G., Kennicutt, R. C., & Whitmore, B. 2010, *ApJ*, 719, L158
- Campbell, M. A., Evans, C. J., Mackey, A. D., Gieles, M., Alves, J., Ascenso, J., Bastian, N., & Longmore, A. J. 2010, *MNRAS*, 405, 421
- Caplan, J. & Deharveng, L. 1986, *A&A*, 155, 297
- Ciardullo, R., Jacoby, G. H., Ford, H. C., & Neill, J. D. 1989, *ApJ*, 339, 53
- Devereux, N. A., Price, R., Wells, L. A., & Duric, N. 1994, *AJ*, 108, 1667
- Elmegreen, B. G. & Hunter, D. A. 2000, *ApJ*, 540, 814
- Esteban, C., Bresolin, F., Peimbert, M., García-Rojas, J., Peimbert, A., & Mesa-Delgado, A. 2009, *ApJ*, 700, 654
- Fardal, M. A., Babul, A., Guhathakurta, P., Gilbert, K. M., & Dodge, C. 2008, *ApJ*, 682, L33
- Feinstein, C. 1997, *ApJS*, 112, 29

- Galarza, V. C., Walterbos, R. A. M., & Braun, R. 1999, *AJ*, 118, 2775
- Giammanco, C., Beckman, J. E., Zurita, A., & Relaño, M. 2004, *A&A*, 424, 877
- Gonzalez Delgado, R. M. & Perez, E. 1997, *ApJS*, 108, 199
- Gordon, K. D., Bailin, J., Engelbracht, C. W., Rieke, G. H., Misselt, K. A., Latter, W. B., Young, E. T., Ashby, M. L. N., Barmby, P., Gibson, B. K., Hines, D. C., Hinz, J., Krause, O., Levine, D. A., Marleau, F. R., Noriega-Crespo, A., Stolovy, S., Thilker, D. A., & Werner, M. W. 2006, *ApJ*, 638, L87
- Greenawalt, B., Walterbos, R. A. M., & Braun, R. 1997a, *ApJ*, 483, 666
- . 1997b, *ApJ*, 483, 666
- Gutiérrez, L., Beckman, J. E., & Buenrostro, V. 2011, *AJ*, 141, 113
- Halliday, C., Carter, D., Bridges, T. J., Jackson, Z. C., Wilkinson, M. I., Quinn, D. P., Evans, N. W., Douglas, N. G., Merrett, H. R., Merrifield, M. R., Romanowsky, A. J., Kuijken, K., & Irwin, M. J. 2006, *MNRAS*, 369, 97
- Hodge, P., Krienke, O. K., Bianchi, L., Massey, P., & Olsen, K. 2010, *PASP*, 122, 745
- Hodge, P. & Lee, M. G. 1990, *PASP*, 102, 26
- Hodge, P., Lee, M. G., & Gurwell, M. 1990, *PASP*, 102, 1245
- Hodge, P. W. & Kennicutt, Jr., R. C. 1983, *ApJ*, 267, 563
- Hodge, P. W., Krienke, O. K., Bellazzini, M., Perina, S., Barmby, P., Cohen, J. G., Puzia, T. H., & Strader, J. 2009, *AJ*, 138, 770
- Ibata, R., Irwin, M., Lewis, G., Ferguson, A. M. N., & Tanvir, N. 2001, *Nature*, 412, 49
- James, P. A., Shane, N. S., Beckman, J. E., Cardwell, A., Collins, C. A., Etherton, J., de Jong, R. S., Fathi, K., Knapen, J. H., Peletier, R. F., Percival, S. M., Pollacco, D. L., Seigar, M. S., Stedman, S., & Steele, I. A. 2004, *A&A*, 414, 23
- James, P. A., Shane, N. S., Knapen, J. H., Etherton, J., & Percival, S. M. 2005, *A&A*, 429, 851
- Kang, Y., Bianchi, L., & Rey, S. 2009, *ApJ*, 703, 614
- Kennicutt, R. C., Hao, C., Calzetti, D., Moustakas, J., Dale, D. A., Bendo, G., Engelbracht, C. W., Johnson, B. D., & Lee, J. C. 2009, *ApJ*, 703, 1672

- Kennicutt, Jr., R. C. 1984, *ApJ*, 287, 116
- . 1988, *ApJ*, 334, 144
- . 1998, *ARA&A*, 36, 189
- Kennicutt, Jr., R. C., Edgar, B. K., & Hodge, P. W. 1989, *ApJ*, 337, 761
- Kennicutt, Jr., R. C., Lee, J. C., Funes, José G., S. J., Sakai, S., & Akiyama, S. 2008, *ApJS*, 178, 247
- Knapen, J. H. 1998, *MNRAS*, 297, 255
- Knapen, J. H., Arnth-Jensen, N., Cepa, J., & Beckman, J. E. 1993, *AJ*, 106, 56
- Knapen, J. H., Stedman, S., Bramich, D. M., Folkes, S. L., & Bradley, T. R. 2004, *A&A*, 426, 1135
- Krienke, O. K. & Hodge, P. W. 2007, *PASP*, 119, 7
- Krumholz, M. R. & McKee, C. F. 2008, *Nature*, 451, 1082
- Lawton, B., Gordon, K. D., Babler, B., Block, M., Bolatto, A. D., Bracker, S., Carlson, L. R., Engelbracht, C. W., Hora, J. L., Indebetouw, R., Madden, S. C., Meade, M., Meixner, M., Misselt, K., Oey, M. S., Oliveira, J. M., Robitaille, T., Sewilo, M., Shiao, B., Vijh, U. P., & Whitney, B. 2010, *ApJ*, 716, 453
- Massey, P., McNeill, R. T., Olsen, K. A. G., Hodge, P. W., Blaha, C., Jacoby, G. H., Smith, R. C., & Strong, S. B. 2007, *AJ*, 134, 2474
- Massey, P., Olsen, K. A. G., Hodge, P. W., Strong, S. B., Jacoby, G. H., Schlingman, W., & Smith, R. C. 2006, *AJ*, 131, 2478
- McConnachie, A. W., Irwin, M. J., Ibata, R. A., Dubinski, J., Widrow, L. M., Martin, N. F., Côté, P., Dotter, A. L., Navarro, J. F., Ferguson, A. M. N., Puzia, T. H., Lewis, G. F., Babul, A., Barmby, P., Bienaymé, O., Chapman, S. C., Cockcroft, R., Collins, M. L. M., Fardal, M. A., Harris, W. E., Huxor, A., Mackey, A. D., Peñarrubia, J., Rich, R. M., Richer, H. B., Siebert, A., Tanvir, N., Valls-Gabaud, D., & Venn, K. A. 2009, *Nature*, 461, 66
- Merrett, H. R., Merrifield, M. R., Douglas, N. G., Kuijken, K., Romanowsky, A. J., Napolitano, N. R., Arnaboldi, M., Capaccioli, M., Freeman, K. C., Gerhard, O., Coccato, L., Carter, D., Evans, N. W., Wilkinson, M. I., Halliday, C., & Bridges, T. J. 2006, *MNRAS*, 369, 120

- Meurer, G. R., Wong, O. I., Kim, J. H., Hanish, D. J., Heckman, T. M., Werk, J., Bland-Hawthorn, J., Dopita, M. A., Zwaan, M. A., Koribalski, B., Seibert, M., Thilker, D. A., Ferguson, H. C., Webster, R. L., Putman, M. E., Knezek, P. M., Doyle, M. T., Drinkwater, M. J., Hoopes, C. G., Kilborn, V. A., Meyer, M., Ryan-Weber, E. V., Smith, R. C., & Staveley-Smith, L. 2009, *ApJ*, 695, 765
- Meyssonnier, N., Lequeux, J., & Azzopardi, M. 1993, *A&AS*, 102, 251
- Mochejska, B. J., Macri, L. M., Sasselov, D. D., & Stanek, K. Z. 2000, *AJ*, 120, 810
- Montalto, M., Seitz, S., Riffeser, A., Hopp, U., Lee, C., & Schönrich, R. 2009, *A&A*, 507, 283
- Oey, M. S. & Clarke, C. J. 1998, *AJ*, 115, 1543
- Oey, M. S., Parker, J. S., Mikles, V. J., & Zhang, X. 2003, *AJ*, 126, 2317
- Pellet, A., Astier, N., Viale, A., Courtes, G., Maucherat, A., Monnet, G., & Simien, F. 1978, *A&AS*, 31, 439
- Perina, S., Cohen, J. G., Barmby, P., Beasley, M. A., Bellazzini, M., Brodie, J. P., Federici, L., Fusi Pecci, F., Galleti, S., Hodge, P. W., Huchra, J. P., Kissler-Patig, M., Puzia, T. H., & Strader, J. 2010, *A&A*, 511, A23+
- Petit, H., Figon, P., & Petit, M. 1998, *A&AS*, 131, 319
- Pleuss, P. O., Heller, C. H., & Fricke, K. J. 2000, *A&A*, 361, 913
- Rand, R. J. 1992, *AJ*, 103, 815
- Relaño, M. & Kennicutt, R. C. 2009, *ApJ*, 699, 1125
- Rozas, M., Beckman, J. E., & Knapen, J. H. 1996, *A&A*, 307, 735
- Rozas, M., Zurita, A., Heller, C. H., & Beckman, J. E. 1999, *A&AS*, 135, 145
- Salpeter, E. E. 1955, *ApJ*, 121, 161
- Schraml, J. & Mezger, P. G. 1969, *ApJ*, 156, 269
- Schruba, A., Leroy, A. K., Walter, F., Sandstrom, K., & Rosolowsky, E. 2010, *ApJ*, 722, 1699
- Scoville, N. Z., Polletta, M., Ewald, S., Stolovy, S. R., Thompson, R., & Rieke, M. 2001, *AJ*, 122, 3017

- Spitzer, L. 1978, *Physical processes in the interstellar medium* (New York: Wiley-Interscience)
- Tabatabaei, F. S. & Berkhuijsen, E. M. 2010, *A&A*, 517, A77+
- Thilker, D. A., Braun, R., & Walterbos, R. A. M. 2000, *AJ*, 120, 3070
- Thilker, D. A., Walterbos, R. A. M., Braun, R., & Hoopes, C. G. 2002, *AJ*, 124, 3118
- van den Bergh, S. 1981, *AJ*, 86, 1464
- Walterbos, R. A. M. & Braun, R. 1992, *A&AS*, 92, 625
- . 1994, *ApJ*, 431, 156
- Williams, B. F. 2003, *AJ*, 126, 1312
- Youngblood, A. J. & Hunter, D. A. 1999, *ApJ*, 519, 55